

**High-pressure diffraction studies on  $\text{Ca}_2\text{RuO}_4$** P. Steffens,<sup>1</sup> O. Friedt,<sup>1,2</sup> P. Alireza,<sup>3</sup> W. G. Marshall,<sup>4</sup> W. Schmidt,<sup>5</sup> F. Nakamura,<sup>6</sup> S. Nakatsuji,<sup>7</sup> Y. Maeno,<sup>7</sup>  
R. Lengsdorf,<sup>1</sup> M. M. Abd-Elmeguid,<sup>1</sup> and M. Braden<sup>1</sup><sup>1</sup>*II. Physikalisches Institut, Universität zu Köln, Zùlpicher Str. 77, D-50937 Köln, Germany*<sup>2</sup>*Laboratoire Léon Brillouin, C.E.A./C.N.R.S., F-91191 Gif-sur-Yvette CEDEX, France*<sup>3</sup>*Cavendish Laboratory, University of Cambridge, Madingley Road CB3 0HE, Cambridge, United Kingdom*<sup>4</sup>*ISIS Facility, Rutherford Appleton Laboratory, Chilton, Didcot, Oxon OX11 0QX, United Kingdom*<sup>5</sup>*ILL, 6 Rue Jules Horowitz BP 156, 38042 Grenoble CEDEX 9, France*<sup>6</sup>*Department of Quantum Matter, ADSM, Hiroshima University, Higashi-Hiroshima 739-8530, Japan*<sup>7</sup>*Department of Physics, Kyoto University, Kyoto 606-8502, Japan*

(Received 14 February 2005; published 7 September 2005)

We studied the crystal and magnetic structure of  $\text{Ca}_2\text{RuO}_4$  as function of pressure with different diffraction techniques. The first-order phase transition observed at a moderate pressure of  $P=0.5$  GPa between the insulating and the metallic high-pressure phase is characterized by a broad region of phase coexistence. The following structural changes are observed as function of pressure: (a) A discontinuous change of both the tilt and rotational angle of the  $\text{RuO}_6$ -octahedra at this transition, (b) a gradual decrease of the tilt angle in the high-pressure phase ( $P>0.5$  GPa), and (c) the disappearance of the tilt above 5.5 GPa leading to a higher symmetry structure. The magnetism was studied by single-crystal neutron diffraction: The ferromagnetic component of the high-pressure phase and a rearrangement of antiferromagnetic order in the low-pressure phase have been observed.

DOI: [10.1103/PhysRevB.72.094104](https://doi.org/10.1103/PhysRevB.72.094104)

PACS number(s): 61.50.Ks, 74.70.Pq, 61.12.-q, 75.50.Ee

**I. INTRODUCTION**

A wide variety of physical phenomena occur in the single-layered ruthenates and provide an interesting opportunity to study competing ground states and the interplay of structural, magnetic, and transport properties. The unconventional superconductor  $\text{Sr}_2\text{RuO}_4$  possesses the ideal  $\text{K}_2\text{NiF}_4$  structure. The isovalent substitution of  $\text{Ca}^{2+}$  by  $\text{Sr}^{2+}$  leads to a variety of electronic and magnetic phases<sup>1,2</sup> and finally to  $\text{Ca}_2\text{RuO}_4$ —a Mott insulator with antiferromagnetic order ( $T_N=112$  K) at low temperature.<sup>3–6</sup>

Under ambient conditions, a metal-insulator transition to a metallic phase occurs in  $\text{Ca}_2\text{RuO}_4$  when heating above  $T=357$  K. The insulating phase in  $\text{Ca}_2\text{RuO}_4$  can also be suppressed by applying moderate pressure:<sup>7</sup> At room temperature,  $\text{Ca}_2\text{RuO}_4$  becomes metallic at about 0.5 GPa. At slightly higher pressure, it stays metallic down to lowest temperatures and exhibits ferromagnetic order below  $T\approx 10$  K. The Mott transition coincides in both cases—i.e., as function of temperature and of pressure—with a structural transition. The electronic structure of  $\text{Ca}_2\text{RuO}_4$ , i.e., its orbital occupation in the insulating as well as in the metallic phase, is still under debate.<sup>8–13</sup> Due to the crossover from antiferro- to ferromagnetism as function of applied pressure, the high-pressure phase of  $\text{Ca}_2\text{RuO}_4$  is of particular interest. It provides the possibility to study the interplay between structural and magnetic degrees of freedom. In addition, the understanding of the ferromagnetic phase of  $\text{Ca}_2\text{RuO}_4$  might also be helpful in explaining the behavior of  $\text{Ca}_{2-x}\text{Sr}_x\text{RuO}_4$ , which for  $0.2 < x < 0.5$  exhibits metamagnetism and an almost ferromagnetic state near  $x=0.5$ .<sup>14</sup> The analysis of our neutron and x-ray diffraction data solves the high-pressure

crystal structure of  $\text{Ca}_2\text{RuO}_4$  and yields a description of the magnetic order in this compound.

**II. EXPERIMENT**

For the determination of the equation of state, powder samples of  $\text{Ca}_2\text{RuO}_4$  have been studied at the synchrotron beamline F3 at HASYLAB in Hamburg and at the 3T.1 diffractometer at LLB, Saclay. At 3T.1, we used helium gas pressure cells with a maximum pressure of 0.6 GPa, and a constant incident wavelength  $\lambda=2.38$  Å. At the F3 beamline, diamond anvil cells (Bridgman type, 0.6 mm diameter, pressure medium liquid nitrogen) have been used and the lattice constants have been calculated from the peak positions in the energy dispersive powder diffraction spectra. This experiment covers the pressure region up to 15 GPa.

For the detailed structural analysis, Rietveld refinable powder data have been collected using the PEARL/HiPr time-of-flight diffractometer at ISIS up to a pressure of almost 10 GPa (Paris–Edinburgh cell). The pressure has been obtained with a fit of the lattice constants to the equation of state (Fig. 1) since in this setup the pressure has not been measured directly. All measurements have been performed at room temperature.

In addition, elastic neutron scattering data at high pressure have been obtained from two single crystals using the IN12 triple-axis spectrometer with a clamp pressure cell at ILL in Grenoble. These measurements have been performed between 1.5 K and room temperature in (100)-(010) and (100)-(001) geometry (scattering plane), respectively. The volume of the crystals was only a few  $\text{mm}^3$ . Until now, larger  $\text{Ca}_2\text{RuO}_4$  single crystals are generally not available because

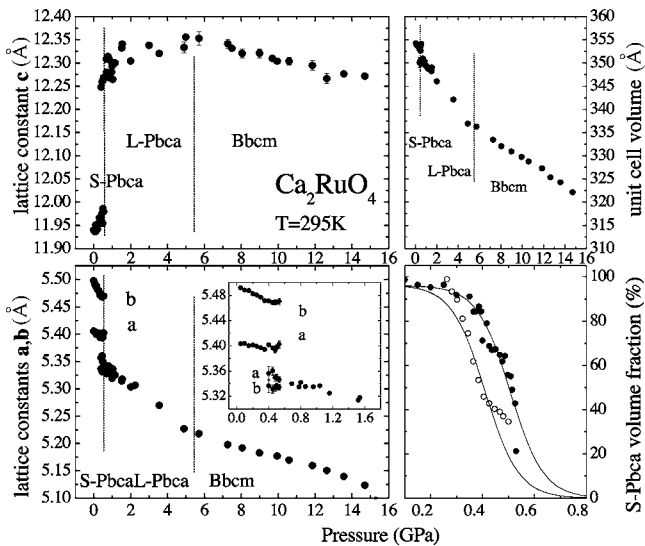


FIG. 1. Left: Pressure dependence of the lattice constants of  $\text{Ca}_2\text{RuO}_4$ . Data were taken by neutron (up to 1 GPa only) and synchrotron powder diffraction (whole pressure range). The inset shows  $a$  and  $b$  near the phase transition from S-Pbca to L-Pbca. Upper right: Evolution of the unit-cell volume. Lower right: Hysteresis of the S-Pbca volume fraction at the transition. The corresponding space groups are indicated, and the phase transitions are marked by dashed lines.

of the discontinuous and hence destructive structural transition at 357 K. The triple-axis spectrometer IN12 allowed us to significantly reduce the high background caused by the pressure cell.

### III. RESULTS AND DISCUSSION

#### A. Pressure dependence of the crystal structure at room temperature

As the first step of the structural analysis, the pressure dependence of the lattice constants, i.e., the equation of state, has been determined up to 15 GPa. The results are shown in Fig. 1. At 0.5 GPa, the discontinuous transition from the S-Pbca into the L-Pbca phase takes place (see upper part of Fig. 1). These phases are named according to the short respectively, long lattice constant  $c$ . Our structural analysis (see below) shows that these phases and the transition between them are the same as in the phase diagram of  $\text{Ca}_{2-x}\text{Sr}_x\text{RuO}_4$ ,<sup>2,5</sup> where this transition is observed as function of  $x$  and  $T$  (at 357 K in  $\text{Ca}_2\text{RuO}_4$ ). The transition is of first order, and as function of pressure it has a hysteresis of  $\sim 0.1$  GPa. At the pressure-driven transition, the lattice volume decreases by about 0.85%, i.e., only slightly more than at the temperature-driven transition under ambient pressure.<sup>2</sup> This transition has to be regarded as just the same transition as the temperature-driven one. It is susceptible to pressure because of its negative volume change.

Above the first-order transition, the orthorhombic splitting has the opposite sign ( $a > b$ ) and is so small that it could only be detected in the PEARL/HiPr neutron diffraction experiment and not in the synchrotron spectra. The neutron

diffraction data yield a splitting of  $(a-b)/(a+b)$  around  $10^{-3}$ . Although it is obvious that pressure stabilizes the state with lower volume, the discontinuous increase of  $c$  and the positive  $\partial c/\partial P$  over a wide pressure range are remarkable.

The results of the full structure refinements of the PEARL/HiPr data are given in Table I. The programs GSAS (Ref. 15) and Fullprof (Ref. 16) have been used for the refinement, and the results cross checked for consistency. During the refinement, special attention was paid to the determination of the characteristic structural distortions, i.e., the  $\text{RuO}_6$ -octahedra's angle of rotation around their vertical axis ( $\parallel c$ ),  $\Phi$ , and the tilt angle  $\Theta$  around an axis in the basal plane ( $\parallel b$ , and parallel to two of the O–O bonds; for further details see Ref. 2). The results are summarized in Fig. 2.

In the high-pressure region, where the tilt distortion is only small, we have described the spectra with different structural models: One in which a tilt of the octahedra, caused by a nonzero  $z$  position of the O(1)-atom (basal oxygen) and nonzero  $x$  and  $y$  of O(2) (apical oxygen), was allowed (space group Pbca). In the other model (space group Bbcm), the nonzero positions were forbidden.

Above 7 GPa, the  $R$  values of both fits differ so little that the lower symmetry is not justified. It has also been possible to fix the horizontal Ca positions to zero without affecting the quality of the fit. In contrast, at pressures lower than 5 GPa, satisfactory descriptions can only be obtained in the usual Pbca symmetry. At 5 GPa, the difference between the two models is only small, but the calculated angle of rotation  $\Phi$  and tilt angle  $\Theta$  are still significantly above zero.

With respect to Fig. 1, one may argue that the lattice constants  $a$ ,  $b$ , and  $c$ , and the cell volume display an anomaly between 5 and 6 GPa: A maximum in  $c$  and a kink in  $a$ ,  $b$ , and  $V$ . Below, the compressibility is  $-(1/V)(\partial V/\partial P) = 9.0 \times 10^{-3} \text{ GPa}^{-1}$ , and above, it is only  $4.6 \times 10^{-3} \text{ GPa}^{-1}$ . This behavior is qualitatively similar to the one observed when heating above 650 K (Ref. 17) under ambient pressure, see Fig. 3. Here,  $\text{Ca}_2\text{RuO}_4$  undergoes a second structural transition to a higher symmetry phase characterized by the suppression of the octahedra's tilt. Having the analogy in mind, one may precisely determine the pressure at which the phase transition occurs from the pressure dependence of the lattice constants (see Fig. 1). We conclude that the tilt vanishes at  $\sim 5.5$  GPa, and that  $\text{Ca}_2\text{RuO}_4$  undergoes a continuous phase transition to a phase with space group Bbcm (standard setting  $Acam$ ). The latter is characterized by a rotation of the  $\text{RuO}_6$ -octahedra around the vertical axis only. This distortion pattern is also found in  $\text{Gd}_2\text{CuO}_4$ .<sup>18</sup> Note that the space group of this phase has to be distinguished from the tetragonal space group  $I4_1/acd$ , which is found<sup>2</sup> in  $\text{Ca}_{2-x}\text{Sr}_x\text{RuO}_4$  and which is also characterized by the  $\text{RuO}_6$  octahedra's rotation around  $c$ , because the sense of the rotation with respect to second-nearest-neighbor planes is different. (This results in a lattice constant  $c$  which is twice as long in the  $I4_1/acd$  phase,  $c \approx 25 \text{ \AA}$ , compared to Bbcm and Pbca with  $c \approx 12.5 \text{ \AA}$ .) Furthermore, in the orthorhombic space group Bbcm, a very small orthorhombic splitting seems to remain. Due to the absence of the tilt, this reflects a deformation of the basal plane of the octahedron. The Bbcm symmetry also allows for a splitting of the in-plane Ru–O bond lengths. Whether this is the case, could not unambigu-

TABLE I. Results of the room-temperature structure refinements of  $\text{Ca}_2\text{RuO}_4$  under pressure at the PEARL/HiPr beamline (ISIS). Errors of the last digit are given in parentheses and represent only statistical errors, not systematic errors which may for instance arise from correlations between parameters. The position of the Ru atom is always (0, 0, 0). Anisotropic thermal parameters could not be refined, therefore only the  $U_{\text{iso}}$  are given. The  $x$  and  $y$  positions of O(1) were constrained in the way that all Ru-O(1) bonds are equal.

$P$ (GPa)	0.1	0.3	1	3	5	7.5	9.7
Space group	S-Pbca	S-Pbca	L-Pbca	L-Pbca	L-Pbca	Bbcm	Bbcm
$a$ (Å)	5.4044(6)	5.4006(5)	5.3312(6)	5.2817(6)	5.2266(9)	5.2020(6)	5.1859(6)
$b$ (Å)	5.4904(6)	5.4760(5)	5.3160(6)	5.2689(5)	5.2187(9)	5.1865(6)	5.1673(6)
$c$ (Å)	11.9507(10)	11.9664(9)	12.2923(8)	12.3354(5)	12.3541(6)	12.3301(6)	12.3078(6)
$R_{wp}$ (%)	3.33	3.07	2.70	2.25	2.72	2.40	2.39
<b>Ca</b> $x$	0.0108(13)	0.0092(13)	0.0116(13)	0.0109(14)	-0.001(2)	0	0
$y$	0.0456(12)	0.0463(12)	0.0289(15)	0.0155(19)	0.016(2)	0	0
$z$	0.3492(5)	0.3484(5)	0.3473(4)	0.3461(3)	0.3463(3)	0.3457(3)	0.3451(3)
$U_{\text{iso}}$ (Å <sup>2</sup> )	0.0102(15)	0.0145(17)	0.0107(11)	0.0118(10)	0.0065(11)	0.0083(8)	0.0093(8)
<b>Ru</b> $U_{\text{iso}}$ (Å <sup>2</sup> )	0.0024(10)	0.0013(8)	0.0011(7)	0.0020(6)	0.0018(8)	0.0032(7)	0.0040(8)
<b>O(1)</b> $x$	0.1953(6)	0.1966(6)	0.1909(4)	0.1894(3)	0.1847(4)	0.1851(4)	0.1832(4)
$y$	0.3030(6)	0.3019(6)	0.3094(4)	0.3110(3)	0.3155(4)	0.3153(4)	0.3173(4)
$z$	0.0244(4)	0.0238(4)	0.0134(4)	0.0101(4)	0.0039(10)	0	0
$U_{\text{iso}}$ (Å <sup>2</sup> )	0.0082(10)	0.0080(9)	0.0077(8)	0.0070(7)	0.0058(7)	0.0071(6)	0.0070(6)
<b>O(2)</b> $x$	-0.0602(7)	-0.0589(7)	-0.0385(8)	-0.0283(9)	-0.0163(17)	0	0
$y$	-0.0201(10)	-0.0186(10)	-0.0116(12)	-0.0103(13)	-0.004(2)	0	0
$z$	0.1657(4)	0.1660(4)	0.1662(3)	0.1666(2)	0.1667(3)	0.1661(2)	0.1667(2)
$U_{\text{iso}}$ (Å <sup>2</sup> )	0.0081(11)	0.0098(11)	0.0092(10)	0.0091(8)	0.0084(8)	0.0095(6)	0.0095(6)
Ru-O(1) (Å)	1.991(3)	1.985(3)	1.941(2)	1.924(2)	1.909(2)	1.898(2)	1.895(2)
Ru-O(2) (Å)	2.010(5)	2.015(5)	2.054(4)	2.062(3)	2.062(3)	2.048(3)	2.052(3)
O(1)-O(1) $\parallel a$ (Å)	2.825(5)	2.818(4)	2.759(3)	2.729(3)	2.703(3)	2.688(3)	2.685(3)
O(1)-O(1) $\parallel b$ (Å)	2.808(5)	2.798(4)	2.732(3)	2.711(3)	2.697(3)	2.680(3)	2.675(3)
$\Theta(O1)$	12.0(2)	11.7(2)	7.0(2)	5.3(2)	2.0(5)	—	—
$\Theta(O2)$	9.83(12)	9.55(11)	5.99(12)	4.4(2)	2.4(3)	—	—
$\Phi$	12.15(9)	11.89(9)	13.33(7)	13.67(5)	14.67(6)	14.59(5)	15.02(5)

ously be determined.<sup>24</sup> In contrast to the tilt, the rotational distortion is not suppressed by pressure; it even increases slightly (Fig. 2).

The uncommon behavior of the lattice constant  $c$  is reflected in the bond length between Ru and O(2), which increases with increasing pressure up to 5 GPa, while the Ru-O(1) bond length decreases continuously. This effect is correlated to the pressure dependence of the resistivity  $\rho_{ab}$  and  $\rho_c$  ( $\rho_c$  increases,  $\rho_{ab}$  decreases with  $P$ ).<sup>7</sup> The overlap of the in-plane orbitals corresponds to the usual effect of pressure, i.e., it is enhanced and may explain the higher conductivity.

It is tempting to interpret the pressure dependencies of the structural parameters and of the magnetism in  $\text{Ca}_2\text{RuO}_4$  in view of calculations that have been carried out for the  $\text{Ca}_{2-x}\text{Sr}_x\text{RuO}_4$  phase diagram.<sup>8,9</sup> Nakamura *et al.*<sup>7</sup> determined with their experiment the evolution of the ferromagnetic ordering temperature (partly deduced from resistivity measurements) with pressure,  $T_C(P)$ .  $T_C(P)$  increases from 10 K just above the phase transition at  $\sim 0.5$  GPa to a maximum value of 25 K at  $\sim 5$  GPa, i.e., the pressure dependencies of  $T_C(P)$  and the tilt angle  $\Theta$  coincide such that with

increasing pressure  $T_C(P)$  increases while  $\Theta$  decreases, and when  $T_C(P)$  peaks the tilt  $\Theta$  disappears.

Fang and Terakura<sup>9</sup> performed calculations considering the influence of structural distortions on the magnetic properties. They find that the octahedral rotation favors a ferromagnetic ground state due to the smaller width of the Ru  $d_{xy}$  band, whereas the tilting has the opposite effect. This goes well with the fact that the ordering temperature is maximum at the same pressure as the tilt disappears (at 300 K). On the other hand, our structural analysis shows that below 5 GPa there are relatively large tilt angles which obviously do not prevent (ferro-)magnetic order. Near  $T_C$ , i.e., at low temperature we even expect the tilt angle to be significantly larger; however, the structure has not yet been determined at low temperature and such a pressure.

The occurrence of ferromagnetism in the tilt distorted structure is remarkable in view of the phase diagram of  $\text{Ca}_{2-x}\text{Sr}_x\text{RuO}_4$ . There, the tilt of the octahedron sets in below a critical Sr-concentration,  $x=0.5$ , which induces antiferromagnetic correlations. In this case, the tilt appears to drive the system very rapidly away from the ferromagnetic instability.<sup>1,2</sup>

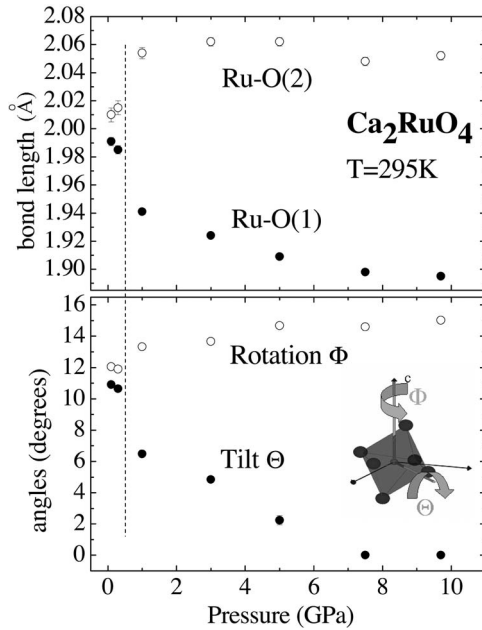


FIG. 2. Top: Evolution of the Ru–O bond lengths. Lower panel: Rotation and tilt angles of the  $\text{RuO}_6$ -octahedra. The tilt angle shown is the average of  $\Theta(\text{O}2)$  and  $\Theta(\text{O}1)$ . (Note that the pressure range is smaller than in Fig. 1.)

## B. Temperature dependence of the crystal structure under pressure

### 1. The two phase region

The lattice constants of a single crystal have been measured at a constant pressure of 1 GPa as function of temperature in the metallic and in the insulating phase on the IN12 spectrometer.

At 1 GPa, a single metallic L-Pbca phase exists at room temperature. At low temperatures, the crystal partially transforms back into the insulating S-Pbca phase (see inset of Fig. 4), i.e., there is a coexistence of both phases. At room temperature, the hysteresis as function of pressure is  $\sim 0.1$  GPa (see Fig. 1), and a coexistence of both phases is found between 0.3 and 0.7 GPa. At low temperatures, this region is broader. Raman studies by Snow *et al.*<sup>19</sup> show that the two phase state exists up to  $\sim 1$  GPa. Measurements of magnetization and resistivity<sup>20</sup> indicate that small amounts of the insulating phase persist even up to  $\sim 2$  GPa. In the region of coexistence, the lattice constants of both phases could be measured as function of temperature at the constant pressure of about 1 GPa (see Fig. 4).

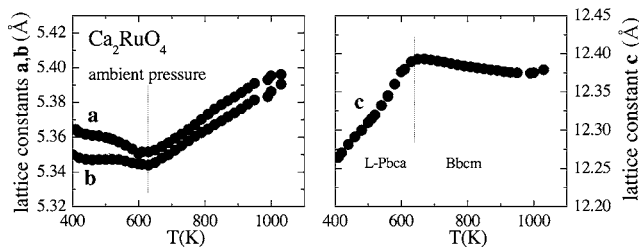


FIG. 3. Temperature dependence of the lattice constants of  $\text{Ca}_2\text{RuO}_4$  at ambient pressure as measured by x-ray diffraction.

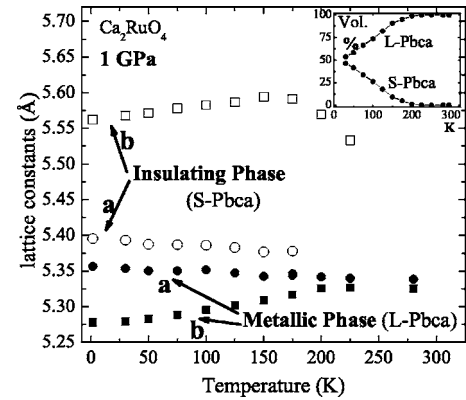


FIG. 4. Temperature dependence of the lattice constants and volume fractions (inset) of both phases at  $P=1$  GPa. All data were obtained on heating. In the mixed state, low temperature stabilizes the S-Pbca phase and the phase transition shifts to higher pressures: At 1 GPa and 1.5 K there is an equal mixture of both phases (inset). Therefore, at low temperature both phases (L- and S-Pbca) could be studied simultaneously and at the same pressure.

### 2. The insulating phase

In comparison to the low temperature lattice constants of  $\text{Ca}_2\text{RuO}_4$  at ambient pressure,  $a=5.38$  Å,  $b=5.63$  Å, the lattice is compressed mainly in  $b$  direction, i.e., the  $\text{RuO}_6$ -octahedra change shape such that the basal planes are less elongated along  $b$ . As mentioned above, Sr doping has qualitatively the same effect. The origin of the maximum at 150 K is not clear. However, the Néel temperature of the pressurized antiferromagnetic insulating phase is about 150 K (see below).

### 3. The metallic phase

In the context of ferromagnetic order, the discussion of the lattice constants of the metallic phase appears to be very interesting. At room temperature,  $a$  and  $b$  are almost identical, but with decreasing temperature a large and unexpected orthorhombic splitting emerges<sup>26</sup> (see Fig. 4). This splitting points to a lattice distortion which needs further investigation.

### C. Magnetism in the metallic (high-pressure) phase

In the metallic high-pressure phase of  $\text{Ca}_2\text{RuO}_4$ , the remnant magnetization is of the order of  $0.4\mu_B$  per Ru (with  $M\parallel a$ ).<sup>7,20</sup> We searched for scattering arising from magnetic ordering in the metallic phase. Bragg intensities due to ferromagnetic order are on top of the nuclear Bragg reflections; this fact excluded a quantitative determination of the ferromagnetic ordered moment. The (004) reflection has a low nuclear structure factor and, therefore, has the best ratio of magnetic to nuclear intensity. The (004) intensity changes when heating across the magnetic ordering temperature: With the statistics achievable in our measurement, we obtained a decrease of 1.7 times the uncertainty  $\sigma$  of the integrated intensity between 1.5 and 20 K (at a pressure of  $\sim 1.5$  GPa). Within the experimental accuracy, this is consistent with the value of the remnant magnetization.



We also searched for magnetic order at several other positions in reciprocal space. Among the related ruthenates, such as  $\text{Ca}_{2-x}\text{Sr}_x\text{RuO}_4$  and Ti-doped  $\text{Sr}_2\text{RuO}_4$ , very different magnetic instabilities have been found. Ti-doped  $\text{Sr}_2\text{RuO}_4$  exhibits static incommensurate magnetic order<sup>21</sup> at a wave vector  $(0.7, 0.3, 0)$ ; paramagnetic  $\text{Ca}_{1.5}\text{Sr}_{0.5}\text{RuO}_4$  has a very high susceptibility and displays strongly enhanced magnetic fluctuations<sup>22</sup> at  $(0.22, 0, 0)$  as well as at the ferromagnetic zone center.

In contrast to macroscopic experimental methods, the neutron scattering technique allows for the direct observation of other possible types of magnetic order (other than ferromagnetic order) which describe fully or partially the magnetic properties. However, although we measured at these positions and along the high symmetry lines in reciprocal space, neither type of incommensurate or antiferromagnetic order could be detected. We estimate that any long-range order with an ordered moment greater than  $\sim 0.25\mu_B$  would have been detected.

The exclusion of other types of magnetic order is additional support for the conclusion that  $\text{Ca}_2\text{RuO}_4$  orders ferromagnetically. The size of the macroscopic magnetic moment<sup>7</sup> is in agreement with itinerant ferromagnetism but is inconsistent with a weak ferromagnetic component accompanying antiferro or incommensurate magnetic order. The magnetic hysteresis is observed in all lattice directions, and the ordering temperatures are one order of magnitude lower than the Néel temperatures in  $\text{Ca}_2\text{RuO}_4$ . Finally, the temperature dependence of the resistivity indicates two-dimensional itinerant ferromagnetism.<sup>20,23</sup>

Our elastic neutron scattering results support the interpretation that the high-pressure phase of  $\text{Ca}_2\text{RuO}_4$  exhibits itinerant ferromagnetism.

#### D. Magnetism in the insulating (low-pressure) phase

A further result concerns the insulating S-Pbca phase and its antiferromagnetic order ( $T_N=112$  K at  $P=0$  GPa,  $M=1.3\mu_B$ ). We find the ordered moment on the Ru sites to point along the  $b$  direction of the lattice<sup>25</sup> in agreement with the previous results at ambient pressure. Early studies by neutron powder diffraction,<sup>5</sup> however, found a mixture of two different antiferromagnetic phases which differ in the stacking sequence of adjacent layers. This leads either to an A-centered or a B-centered magnetic unit cell.

At ambient pressure, the A-centered type of magnetic order has an ordering temperature of  $T_N=112$  K and has been found to be the majority phase, whereas the minority B phase has the higher  $T_N$ :  $T_N=150$  K. A similar phase mixture has been observed in some other samples, but in all high-quality single crystals only a single transition at 112 K could be detected.<sup>20</sup> The existence of the second phase is most likely caused by small variations in the oxygen content—note that  $\text{Ca}_2\text{RuO}_4$  with excess oxygen has been shown to have *only* the B-centered antiferromagnetic order.<sup>5</sup> Samples containing Sr ( $\text{Ca}_{2-x}\text{Sr}_x\text{RuO}_4$  with  $x \geq 0.03$ ) also exhibit only the B-centered order<sup>2,17</sup> and Néel temperatures of  $\sim 150$  K.

At 1 GPa and 1.5 K, we were not able to detect in either crystal orientation magnetic scattering at Bragg positions

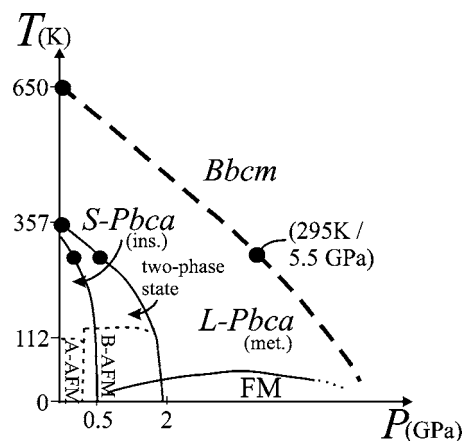


FIG. 5. Schematic structural and magnetic  $P$ - $T$  phase diagram of  $\text{Ca}_2\text{RuO}_4$  (phase boundaries and distances are not true to scale). S-Pbca and L-Pbca denote the structure with tilt distortion (insulating and metallic, respectively) and at the transition a broad region of phase coexistence is found. The phase border to the nontilted Bbcm structure is known at two points only. A-AFM and B-AFM denote antiferromagnetic order with A- and B-centered magnetic unit cell, respectively. FM is the ferromagnetic metallic phase (Ref. 7) with maximum  $T_C$  around 25 K at 5 GPa.

corresponding to the A-centered antiferromagnetic order in the S-Pbca phase. However, we observed magnetic scattering at the  $(012)$ -position, which corresponds to the B-centered type of order. We conclude that there is a single magnetic phase of this type, in contrast to the behavior of the S-Pbca phase at ambient pressure. We have not determined the full temperature dependence of the magnetic scattering corresponding to the B-type antiferromagnetic order, but at  $T \approx 150$  K the magnetic intensities have entirely disappeared. Susceptibility measurements<sup>20</sup> show that  $T_N$  is 145 K at  $P=0.8$  GPa, i.e., nearly the value found in all samples with B-type order at ambient pressure.

The reason for the alteration of the magnetic order from A to B type is not clear, as the coupling between different layers is not yet well understood. However, one may argue that it is the same effect as seen in the Sr-doped samples: The application of pressure and the substitution with small amounts of Sr have a similar effect on the lattice constants and their temperature dependence.<sup>17</sup> Furthermore, in both cases the tilt distortion is suppressed. Hence, the same subtle structural effects may be the reason for the change from A- to B-type order.

#### E. The phase diagram

In Fig. 5, we show a schematic  $P$ - $T$  phase diagram of  $\text{Ca}_2\text{RuO}_4$  which summarizes the results on structure and magnetic order. At ambient pressure,  $\text{Ca}_2\text{RuO}_4$  is an insulator with an A-centered antiferromagnetic unit cell below  $T_N=112$  K. Applying moderate pressure, the magnetic order changes to B-centered antiferromagnetism. The change occurs at a pressure between 0.2 and 0.8 GPa. The B-type order exhibits a higher Néel temperature ( $T_N > 140$  K). Upon increasing temperature or pressure, a first-order structural

phase transition to the L-Pbca phase takes place. This phase is metallic, and it is ferromagnetic at low temperature. The phase transition involves a relatively broad region of phase coexistence—at low temperature it extends from about 0.5 to 2 GPa; this region is marked as “two-phase state”. At even higher temperatures or pressures, the tilt of the octahedra is completely suppressed; the phase transition to the nontilted structure with space group Bbcm takes place at 650 K (ambient pressure) or at 5.5 GPa (room temperature).

#### *Comparison with the phase diagram of $\text{Ca}_{2-x}\text{Sr}_x\text{RuO}_4$*

There are analogies between the application of pressure and the substitution of Ca by Sr: For Sr concentrations of  $0 < x < 0.2$ ,  $x$  and  $T$  drive a first-order transition from an insulating S-Pbca phase (found at low  $x$  and low  $T$ ) to a metallic L-Pbca phase, followed by a second-order phase transition to Bbcm.<sup>1,2,17</sup> Antiferromagnetism in the S-Pbca phase changes from A- to B-centered order upon Sr doping. For  $0 < x < 0.2$ , the  $x$ - $T$  phase diagram is therefore similar to the  $P$ - $T$  phase diagram for pressures below  $\sim 2$  GPa, and the crystal structures are basically identical. However, although higher Sr concentrations finally suppress the tilt down to lowest temperatures, the evolution is different, because in the  $\text{Ca}_{2-x}\text{Sr}_x\text{RuO}_4$  phase diagram the regions  $x < 0.2$  and  $x > 0.2$  are separated by a first-order phase boundary due to different rotation schemes, as discussed above in Sec. III A.

#### IV. CONCLUSION

We have determined the structural properties of  $\text{Ca}_2\text{RuO}_4$  at room temperature up to a pressure of 10 GPa and the lattice constants up to 15 GPa. A first-order structural transition leads from the insulating S-Pbca to the metallic L-Pbca phase and involves a region of phase coexistence. In the metallic phase, the tilt angle is strongly reduced, but still significantly different from zero. Only at much higher pressure (above 5.5 GPa at room temperature) the transition into the higher symmetry Bbcm structure without tilt was observed. In contrast, the rotational distortion is only weakly pressure dependent. In the insulating phase two different types of antiferromagnetic order exist, and pressure seems to control the crossover from A-centered at ambient pressure to B-centered order (with higher Néel temperatures). In the metallic phase, we observed weak Bragg scattering due to ferromagnetism. The surprisingly large orthorhombic splitting at lower temperatures indicates that in this phase further structural effects take place that have not yet been characterized in detail.

#### ACKNOWLEDGMENTS

This work was supported by the Deutsche Forschungsgemeinschaft through SFB 608 and grants from JSPS and MEXT of Japan.

- 
- <sup>1</sup>S. Nakatsuji and Y. Maeno, Phys. Rev. Lett. **84**, 2666 (2000); S. Nakatsuji and Y. Maeno, Phys. Rev. B **62**, 6458 (2000).
- <sup>2</sup>O. Friedt, M. Braden, G. André, P. Adelman, S. Nakatsuji, and Y. Maeno, Phys. Rev. B **63**, 174432 (2001).
- <sup>3</sup>S. Nakatsuji, S. Ikeda, and Y. Maeno, J. Phys. Soc. Jpn. **66**, 1868 (1997).
- <sup>4</sup>C. S. Alexander, G. Cao, V. Dobrosavljevic, S. McCall, J. E. Crow, E. Lochner, and R. P. Guertin, Phys. Rev. B **60**, R8422 (1999).
- <sup>5</sup>M. Braden, G. André, S. Nakatsuji, and Y. Maeno, Phys. Rev. B **58**, 847 (1998).
- <sup>6</sup>G. Cao, S. McCall, M. Shepard, J. E. Crow, and R. P. Guertin, Phys. Rev. B **56**, R2916 (1997).
- <sup>7</sup>F. Nakamura, T. Goko, M. Ito, T. Fujita, S. Nakatsuji, H. Fukazawa, Y. Maeno, P. Alireza, D. Forsythe, and S. R. Julian, Phys. Rev. B **65**, 220402(R) (2002).
- <sup>8</sup>V. I. Anisimov, I. A. Nekrasov, D. E. Kondakov, T. M. Rice, and M. Sigris, Eur. Phys. J. B **25**, 191 (2002).
- <sup>9</sup>Z. Fang and K. Terakura, Phys. Rev. B **64**, 020509(R) (2001); Z. Fang, N. Nagaosa, and K. Terakura, *ibid.* **69**, 045116 (2004).
- <sup>10</sup>T. Hotta and E. Dagotto, Phys. Rev. Lett. **88**, 017201 (2002).
- <sup>11</sup>J. S. Lee, Y. S. Lee, T. W. Noh, S.-J. Oh, Jaejun Yu, S. Nakatsuji, H. Fukazawa, and Y. Maeno, Phys. Rev. Lett. **89**, 257402 (2002).
- <sup>12</sup>J. H. Jung, Z. Fang, J. P. He, Y. Kaneko, Y. Okimoto, and Y. Tokura, Phys. Rev. Lett. **91**, 056403 (2003).
- <sup>13</sup>T. Mizokawa, L. H. Tjeng, G. A. Sawatzky, G. Ghiringhelli, O. Tjernberg, N. B. Brookes, H. Fukazawa, S. Nakatsuji, and Y. Maeno, Phys. Rev. Lett. **87**, 077202 (2001); T. Mizokawa, L. H. Tjeng, H.-J. Lin, C. T. Chen, S. Schuppler, S. Nakatsuji, H. Fukazawa, and Y. Maeno, Phys. Rev. B **69**, 132410 (2004).
- <sup>14</sup>S. Nakatsuji, D. Hall, L. Balicas, Z. Fisk, K. Sugahara, M. Yoshioka, and Y. Maeno, Phys. Rev. Lett. **90**, 137202 (2003).
- <sup>15</sup>A. C. Larson and R. B. von Dreele, Los Alamos National Laboratory Report LAUR 86-748 (2000).
- <sup>16</sup>J. Rodriguez-Carvajal, Physica B **192**, 55 (1993).
- <sup>17</sup>P. Steffens *et al.* (unpublished).
- <sup>18</sup>M. Braden, W. Paulus, A. Cousson, P. Vigoureux, G. Heger, A. Goukassov, P. Bourges, and D. Petitgrand, Europhys. Lett. **25**, 625 (1994).
- <sup>19</sup>C. S. Snow, S. L. Cooper, G. Cao, J. E. Crow, H. Fukazawa, S. Nakatsuji, and Y. Maeno, Phys. Rev. Lett. **89**, 226401 (2002).
- <sup>20</sup>F. Nakamura *et al.* (unpublished).
- <sup>21</sup>M. Braden, O. Friedt, Y. Sidis, P. Bourges, M. Minakata, and Y. Maeno, Phys. Rev. Lett. **88**, 197002 (2002); M. Minakata and Y. Maeno, Phys. Rev. B **63**, 180504(R) (2001).
- <sup>22</sup>O. Friedt, P. Steffens, M. Braden, Y. Sidis, S. Nakatsuji, and Y. Maeno, Phys. Rev. Lett. **93**, 147404 (2004).
- <sup>23</sup>M. Hatatani and T. Moriya, J. Phys. Soc. Jpn. **64**, 3434 (1995).
- <sup>24</sup>An unconstrained shift of the O(1)  $x$  and  $y$  positions can result in two different Ru–O(1) bond lengths. This is an important issue in the discussion of magnetism, because the distortion pattern arising from it could stabilize antiferroorbital order. Unconstrained refinement yields sizeable splittings up to 2%, but the quality of the fit is *not* affected by enforcing the O(1)-shift to be perpendicular to the bond, i.e., a single Ru–O(1) bond length. The table therefore lists the results of the refinement with equal Ru–O(1) bonds. In the case of the S-Pbca structure at ambient

pressure, the same question arises. It could be solved by high resolution powder and single crystal studies: These did not find significant splitting.

<sup>25</sup>Note that due to the rotation of the octahedra, the Ru magnetic moment is also slightly canted away from the crystallographic  $b$  axis.

<sup>26</sup>Here, one has to take into account the possibility, that the phase mixture causes uncontrollable real structure effects which influence the results if the domain sizes are very small. However, we consider this as unlikely, as the analysis of the peak widths did not yield any indication for it. In addition, a similar splitting was observed on different samples.